American Mineralogist, Volume 84, pages 1304–1318, 1999

Hydrothermal synthesis of amphiboles along the tremolite-pargasite join and in the ternary system tremolite-pargasite-cummingtonite

ANURAG SHARMA* AND DAVID M. JENKINS

Department of Geological Sciences and Environmental Studies, Binghamton University, Binghamton, New York 13902-6000, U.S.A.

ABSTRACT

We report here an investigation of amphibole synthesis within the ternary system $Ca_2Mg_5Si_8O_{22}(OH)_2$-$NaCa_2Mg_4Al_3Si_6O_{22}(OH)_2$-$Mg_7Si_8O_{22}(OH)_2$ (= TR-PG-MC) to define better the limits of solid solution for amphiboles formed along and near the join tremolite-pargasite. Hydrothermal syntheses were conducted in the range of 750–1000 °C and 1–6 kbar. Syntheses at 10 mol% compositional intervals along the TR-PG join produced incomplete yields of amphibole, and the resultant amphiboles were found to be associated with varying amounts of accessory clinopyroxene, plagioclase, and gehlenite. Syntheses of end-member pargasite with progressively greater amounts of the MC component produced a very good amphibole yield for a pargasite composition containing 2.5 mol% MC. The persistence of clinopyroxene or gehlenite and the improved yield of pargasitic amphibole with minor addition of the MC component indicate a shift toward MC enrichment for amphiboles made from bulk compositions directly on the TR-PG join. Syntheses within the TR-PG-MC ternary system suggest that the Ca-rich limit of solid solution is a slightly curved field in the TR-PG-MC field. Amphiboles made along this join showed a very systematic change in the (151) and ($\bar{3}$31) peak spacing with mol% PG, providing a simple technique for deducing the composition of amphiboles made near the tremolite-pargasite join. Electron microprobe analysis confirms that the amphiboles for the most part conform to the "pargasite" substitution. The one exception being amphiboles formed near 80–90 mol% PG compositions, which proved both difficult to synthesize (~75 wt% amphibole yield) and displayed a small, but significant, excess of Na in their structure. High yields of amphibole could be formed from this same bulk composition with the use of a dilute NaOH solution instead of pure water, suggesting that there was insufficient Na in the starting mixture to allow complete amphibole formation. Structural refinements using X-ray diffraction (XRD) Rietveld refinement confirmed the high Na content for this sample and also revealed a non-linear trend in the unit-cell volume with composition, with a maximum at the 80 mol% PG bulk composition. The difficulty in synthesizing amphiboles near this bulk composition and its unusually high volume suggest that immiscibility in natural hornblendes may initiate with increasing pressure for pargasite-rich bulk compositions.

INTRODUCTION

The join tremolite [$Ca_2Mg_5Si_8O_{22}(OH)_2$ = TR]-pargasite [$NaCa_2Mg_4Al_3Si_6O_{22}(OH)_2$ = PG] provides a useful first approximation to the (admittedly complex) chemical variation that occurs between actinolite and hornblende, as shown by the amphibole chemistry plots from many meta-mafic rock localities (e.g., Kamineni 1986; Schumacher 1991; Gillis et al. 1993; Lee and Cho 1995). Both end members of this join have been the focus of research in recent years. Tremolite is one of the chemically simplest end-members of the calcic amphiboles and yet a mineral of this ideal composition is not commonly found in nature and has proven difficult, if not impossible, to synthesize (see recent reviews by Maresch et al. 1994; Hawthorne 1995; Yang and Evans 1996; Zimmermann et al. 1996). Cation distribution in synthetic pargasite has been studied recently by Welch et al. (1994) using NMR and IR techniques and by Oberti et al. (1995) using single-crystal XRD analysis. Pargasite has not been so problematic as tremolite to synthesize (e.g., Raudsepp et al. 1991), but it also may display some deviation from its ideal composition as discussed below.

There have been two previous studies devoted to the (Fe-free) tremolite-pargasite join, which were both by Oba (1980, 1990). These studies have focused on establishing the temperature-composition phase equilibria along this join at various pressures. In addition to confirming the higher thermal stability of pargasite relative to tremolite, Oba (1980) reported the presence of an extensive miscibility gap existing along this join at 1 kbar but not at 5 kbar. A second investigation of this join at 10 kbar (Oba 1990) again showed complete miscibility, even at a temperature (800 °C) that was well inside the miscibility gap at 1 kbar. If these results represent true equilibrium, supported by one very long duration (4280 h) compositional re-equilibration experiment at 800 °C and 1 kbar, then one would anticipate immiscibility in hornblendes to be present at pressures below 5 kbar but not above. This pressure

*Present address: Geophysical Laboratory, Carnegie Institute of Washington, 5251 Broad Branch Road, N.W., Washington, D.C. 20015. E-mail: sharma@gl.ciw.edu

0003-004X/99/0009–1304$05.00

dependency in the miscibility gap was supported by Bégin and Carmichael (1992) based on their analysis of coexisting calcic amphiboles in the Cape Smith belt, Québec, and their compilation of data from the literature. A smaller miscibility gap was also observed at 1 kbar by Oba and Yagi (1987) in their study of the actinolite-pargasite join where each end member had 20 mol% Fe^{2+} substituted for Mg^{2+}. They observed that the miscibility gap was much smaller in extent compared to the iron-free system and was displaced noticeably toward the actinolite end member.

Several lines of evidence have prompted us to take a closer look at the synthesis of pargasite and to re-examine amphibole synthesis along the tremolite-pargasite join. First, most of the previous attempts at synthesizing pargasite (Boyd 1959; Charles 1980; Raudsepp et al. 1991; Welch et al. 1994) have produced good but incomplete yields. Typically there are minor amounts (<5%) of extraneous phases present, even after repeated treatments of the same material (Welch et al. 1994). What is curious is that these syntheses always include the Ca-rich phases diopsidic clinopyroxene or gehlenite as the principal accessory phases, suggesting a Ca deficiency in synthetic pargasite analogous to, but not so pronounced as, that observed for synthetic tremolite (e.g., Jenkins 1987). Indeed, we observed diopsidic clinopyroxene coexisting with amphibole for all intermediate bulk compositions along the tremolite-pargasite join, contrary to the results reported by Oba (1980, 1990). Accordingly, we report here our investigation of amphibole synthesis along a portion of the join $NaCa_2Mg_4Al_3Si_6O_{22}(OH)_2$-$Mg_7Si_8O_{22}(OH)_2$ (= PG-MC), along the join $Ca_2Mg_5Si_8O_{22}(OH)_2$-$NaCa_2$ $Mg_4Al_3Si_6O_{22}(OH)_2$ (= TR-PG), and within the ternary system $Ca_2Mg_5Si_8O_{22}(OH)_2$-$NaCa_2Mg_4$ $Al_3Si_6O_{22}(OH)_2$-Mg_7 $Si_8O_{22}(OH)_2$ (= TR-PG-MC). Second, the pressure dependency of the miscibility gap reported by Oba (1980) is counter to that of other miscibility gaps, such as the alkali feldspar join (Luth et al. 1974) and the enstatite-diopside join (Lindsley and Dixon 1976). In support of this unusual pressure dependency, Oba (1980) noted that the molar volume of an amphibole mid-way across this join is slightly smaller than a mechanical mixture of the end members, which would imply an increase in amphibole miscibility with increasing pressure (see below). To corroborate this observation, we report here a detailed analysis of the unit-cell volumes of amphiboles synthesized from bulk compositions within the ternary system TR-PG-MC that produced the highest yields.

Experimental and analytical techniques

Apparatus

All syntheses were performed in internally heated gas vessels using Ar as a pressure medium. Temperatures were measured by two Inconel-sheathed, chromel-alumel thermocouples situated at either end of the sample capsule and calibrated against the freezing points of Sn (231.9 °C), LiCl (605 °C), and NaCl (800.5 °C). The cited temperature uncertainties include thermocouple accuracy (±2 °C), controller variation (±1 °C), and any thermal gradient across the sample. Pressures were monitored with a bourdon-tube gauge and factory-calibrated Harwood manganin cell and are considered accurate to ±50 bars. The cited pressure uncertainties include pressure accuracy and any variation in pressure that might have occurred during the experiment.

Starting material

All synthetic phases were made from mixtures of reagent grade oxides and carbonates. The finely powdered oxides were MgO, which was heated to 900–1000 °C for several hours to drive off any water, CO_2, Al_2O_3 (corundum), and SiO_2 (amorphous silica), which was obtained by heating silicic acid in air at 900–1000 °C for several days. Carbonates were used as sources for Na_2O (Na_2CO_3) and CaO ($CaCO_3$). Dry mixtures having appropriate anhydrous amphibole stoichiometry (Table 1) were prepared by multiple mixings of oxides and carbonates and were heated briefly (30 s) in air to about 1000 °C to drive off CO_2. This process of decarbonation was monitored by checking for stoichiometric CO_2 weight loss. The bulk compositions of the mixtures listed in Table 1 are plotted in Figure 1. For general survey experiments small portions (6–15 mg) of these mixtures were sealed with either distilled water or NaOH solutions in either platinum or gold capsules, the latter being used when corrosion of Pt was observed (most noticeable above 925 °C at 2 kbar). The mass of fluid amounted to 10–40 wt% of the total mass of solid + fluid. Where more accurate Rietveld structural refinements were desired, larger portions (150 mg) of samples were synthesized. Modifications were made to some of the starting mixtures to test the effects of certain chemical changes (i.e., addition of quartz or forsterite) on the yield of amphibole, as discussed below.

Analytical techniques

All experimental products were examined under the petrographic microscope using an oil of refractive index 1.60, which approximately matches the index α of the amphiboles. This

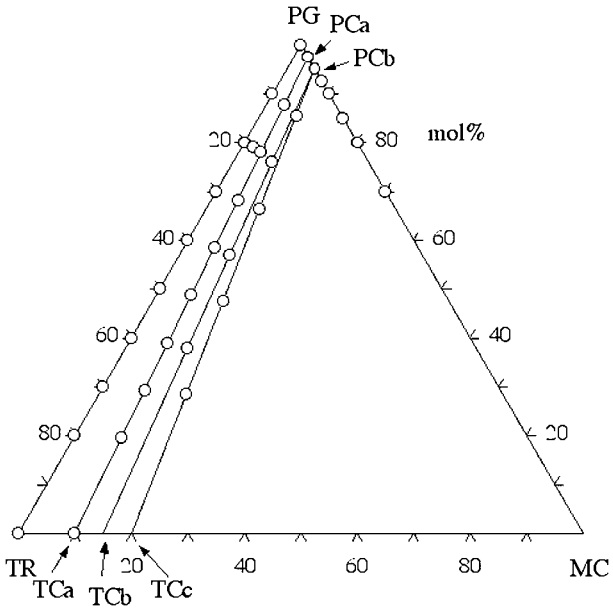

Figure 1. Bulk compositions of starting oxide mixtures in the ternary system $Ca_2Mg_5Si_8O_{22}(OH)_2$ (=TR)-$NaCa_2Mg_4Al_3Si_6O_{22}(OH)_2$ (PG)-$Mg_7Si_8O_{22}(OH)_2$(= MC). Numbers and abbreviations correspond to code prefixes in Table 1.

TABLE 1. Nominal bulk compositions investigated in this study, arranged in approximate order of decreasing PG component

Code prefix	Nominal composition	Components (mol%)
TR	$Ca_2Mg_5Si_8O_{22}(OH)_2$	TR_{100}
PG	$NaCa_2Mg_4Al_3Si_6O_{22}(OH)_2$	PG_{100}
MC	$Mg_7Si_8O_{22}(OH)_2$	MC_{100}
PCa	$Na_{0.975}Ca_{1.95}Mg_{4.075}Al_{2.925}Si_{6.05}O_{22}(OH)_2$	$PG_{97.5}MC_{2.5}$
TCa	$Ca_{1.80}Mg_{5.20}Si_8O_{22}(OH)_2$	$TR_{90}MC_{10}$
PCb	$Na_{0.95}Ca_{1.9}Mg_{4.15}Al_{2.85}Si_{6.1}O_{22}(OH)_2$	$PG_{95}MC_5$
TCb	$Ca_{1.7}Mg_{5.3}Si_8O_{22}(OH)_2$	$TR_{85}MC_{15}$
TCc	$Ca_{1.6}Mg_{5.4}Si_8O_{22}(OH)_2$	$TR_{80}MC_{20}$
PARG 11	$Na_{0.975}Ca_{1.95}Mg_{4.075}Al_{2.925}Si_{6.05}O_{22}(OH)_2$	$PG_{97.5}MC_{2.5}$
PARG 13	$Na_{0.78}Ca_{1.92}Mg_{4.30}Al_{2.34}Si_{6.44}O_{22}(OH)_2$	$PG_{78}TR_{18}MC_4$
PARG 14	$Na_{0.79}Ca_{1.96}Mg_{4.25}Al_{2.37}Si_{6.42}O_{22}(OH)_2$	$PG_{79}TR_{19}$ MC_2
PARG 15	$Na_{0.80}Ca_{2.0}Mg_{4.20}Al_{2.40}Si_{6.40}O_{22}(OH)_2$	$PG_{80}TR_{20}$
PARG 16	$Na_{0.585}Ca_{1.89}Mg_{4.525}Al_{1.755}Si_{6.83}O_{22}(OH)_2$	$PG_{58.5}TR_{36}MC_{5.5}$
PARG 17	$Na_{0.39}Ca_{1.86}Mg_{4.75}Al_{1.17}Si_{7.22}O_{22}(OH)_2$	$PG_{39}TR_{54}$ MC_7
PARG 18	$Na_{0.195}Ca_{1.83}Mg_{4.975}Al_{0.585}Si_{7.61}O_{22}(OH)_2$	$PG_{19.5}TR_{72}MC_{8.5}$
PARG 19	$Na_{0.76}Ca_{1.86}Mg_{4.38}Al_{2.28}Si_{6.48}O_{22}(OH)_2$	$PG_{76}TR_{17}MC_7$
PARG 20	$Na_{0.57}Ca_{1.82}Mg_{4.61}Al_{1.71}Si_{6.86}O_{22}(OH)_2$	$PG_{57}TR_{34}MC_9$
PARG 21	$Na_{0.38}Ca_{1.78}Mg_{4.84}Al_{1.14}Si_{7.24}O_{22}(OH)_2$	$PG_{38}TR_{51}MC_{11}$
TREM 23	$Ca_{1.80}Mg_{5.20}Si_8O_{22}(OH)_2$	$TR_{90}MC_{10}$

made identification of trace amounts of accessory phases particularly easy. In addition to the optical examination, XRD patterns were obtained for all run products to evaluate further the amphibole yield and the nature and approximate concentrations of non-amphibole phases from relative peak heights. Quantitative XRD work was performed on several samples using two different diffractometers. A Scintag XDS-2000 automated diffractometer (Materials Research Center) was used for statistically modeling, using the Pearson VII peak profile, shifts that occur in the $\bar{3}31$ and 151 peak positions with variation in amphibole composition. A Philips PW3040-MPD automated diffractometer was used for performing Rietveld structure refinements. The latter instrument was calibrated using silicon (a_o= 5.4309 Å). Step-scan patterns for Rietveld refinement were collected using fixed 1/2° divergence and anti-scatter slits, 0.2 mm receiving slit, and step intervals of 0.05 °2θ for sufficient durations to obtain approximately 1000–2000 counts on the most intense peaks. Rietveld refinements were performed using the program DBWS-9411 (Young et al. 1994) to obtain structural, chemical, and, where appropriate, modal abundances. Three scans were made of one high-yield amphibole sample by both repacking the sample into the holder ($8 \times 33 \times 1$ mm) as well as removing and remounting the sample holder on the diffractometer between each scan to judge the reproducibility of the derived unit-cell volumes from scan to scan. The derived cell volumes were identical to within $1\sigma = 0.12$ Å^3, which is about the same uncertainty for an individual sample ($1\sigma = 0.09$ Å^3). Details of the refinement procedure followed here are the same as those discussed in Jenkins and Hawthorne (1995).

Chemical analyses of individual synthetic phases were obtained using a JEOL JXA-8900 electron microprobe. Amphiboles with approximately >50 mol% of the PG component were sufficiently thick (5–10 μm) to permit the samples to be epoxy mounted, polished, carbon coated, and analyzed by wavelength dispersive spectroscopy (WDS). Figure 2 is a representative secondary-electron image of amphibole that is formed in this compositional range. Conditions for analysis were 15 kV accelerating potential and 10–20 nA beam current. Amphiboles with approximately <50 mol% of the PG component tended to be thinner than those shown in Figure 2 and did not prove suitable for epoxy mounting. Instead, these samples were dispersed in ethanol, sedimented onto polished graphite stubs, carbon coated, and analyzed by energy-dispersive spectroscopy (EDS) to keep the solid angle of analysis small and thereby minimize topographic artifacts (e.g., Giblin et al. 1993). The Noran Si(Li) EDS detector was operated at a lower accelerating voltage (10 kV) in an attempt to keep more of the excitation volume within the amphibole grain. Analyses were made employing ZAF matrix corrections and using the following standards: albite (Amelia) for Na, MgO for Mg, quartz or diopside for Si, calcite or diopside for Ca, and kyanite for Al. Short counting times (10 s) were used for Na on the albite standard to minimize loss of Na counts via diffusion under the highly focused (spot) beam, made necessary by the thin grains being analyzed; diffusion of Na from the amphibole grains was checked for but not observed. An analysis was deemed acceptable when total cations per 23 oxygen atoms were 15.0–16.0, Ca atoms per formula unit (apfu) were less than 2.05, and analytical totals were 60 wt% or greater. This particular analytical total has been shown to be the approximate minimum that still provides suitable stoichiometries for fine-grained silicates (Solberg et al. 1981; Giblin et al. 1993; Sharma 1996).

X-ray diffraction Δ2θ [(151)-($\bar{3}$31)] analytical procedure

Before continuing the discussion concerning the synthesis of amphiboles along the tremolite-pargasite join, it is shown here that amphibole compositions near the TR-PG join can be

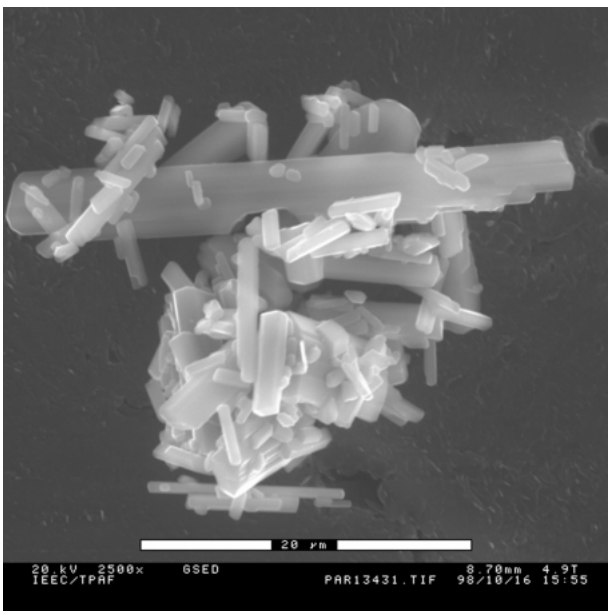

FIGURE 2. Secondary-electron image of sample PARG 13-43 formed at the average conditions of 886 °C and 1.27 kbar for 433 h in 0.5m NaOH solution. Scale bar is 20 μm.

determined quickly using the angular separation of the X-ray reflections 151 and $\bar{3}31$ at ~33.2 and ~32.6 °2θ, respectively. The locations of these X-ray reflections were determined by least-squares fitting of Pearson VII peak profiles to the digitized diffractograms. For the most PG-rich end-member ($PG_{97.5}MC_{2.5}$), these two reflections are 0.75 °2θ apart whereas for the most TR-rich end-member ($TR_{90}MC_{10}$), there is a peak separation of 0.28 °2θ, as shown in Figure 3a. The difference in the peak centroids were correlated empirically with the average microprobe analysis of the amphiboles synthesized for compositions at 10 mol% intervals along the join and this correlation is shown in Figure 3b. Although the correlation is not linear over the whole compositional range, it does involve Bragg peaks that are easily resolved and relatively strong, giving an analytical precision of about ±5 mol% in the middle of the compositional range.

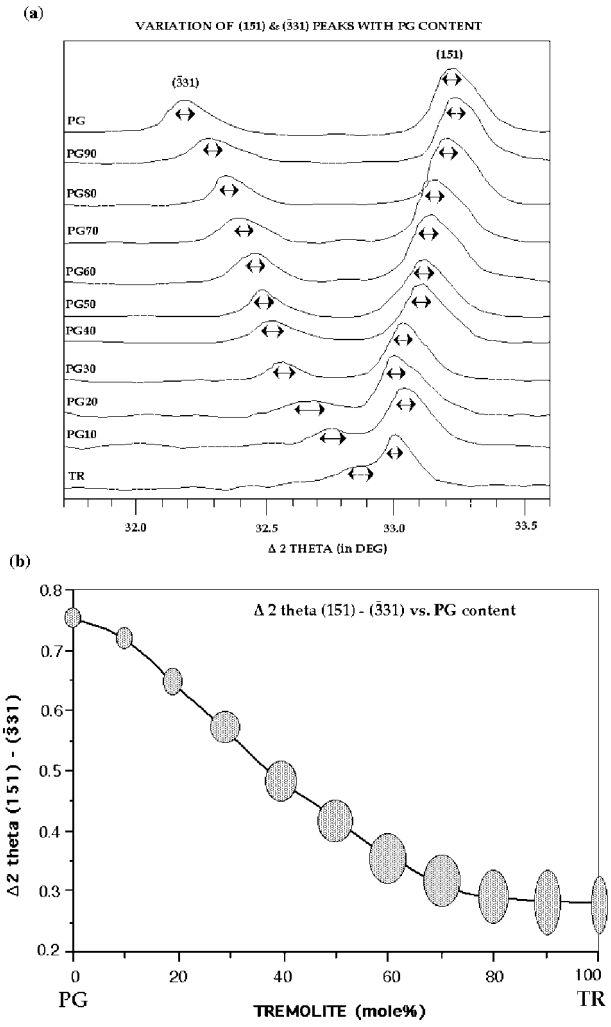

FIGURE 3. (**a**) Portions of the XRD patterns for amphiboles formed at 10 mol% increments along the PG-TR join, indicated by the mol% of PG component on the left. Short double-arrows indicate uncertainty in peak centroid positions for the $\bar{3}31$ and 151 reflections modeled with Pearson VII profiles. (**b**) Difference in the 151 and $\bar{3}31$ X-ray diffraction peaks (Cu*K*α) with change in the bulk TR composition for amphiboles formed along the PG-TR join. Uncertainty is shown by symbol size.

SYNTHESIS RESULTS

Amphibole synthesis attempts along the PG-MC join

Synthesis of pure pargasite was attempted in the range 800 – 950 °C and 3–5 kbar, with the starting compositions and synthesis conditions listed in Tables 1 and 2, respectively. The nucleation of amphibole was rapid, but all the final reaction products indicated the presence of minor (~2–3 wt%) amounts of plagioclase or gehlenite. Presence of these minor Ca- and Al-rich accessory minerals indicate a small shift in the amphibole composition toward Mg and Si enrichment. Multiple retreatments of the runs also gave similar incomplete yields, which indicates conclusion of the reaction.

Several synthesis experiments were performed with varying amounts of MC component added to the pargasite composition to determine the optimal-yield composition. Oxide mixtures were prepared at intervals varying from 2.5 mol% (for PG-rich compositions) to 10 mol% (for MC-rich compositions) and hydrothermally treated at conditions in the range of 800–900 °C and 3–6 kbar. The compositions investigated are listed in Table 1 and the results of the syntheses are listed in Table 2. All the synthesis compositions ranging from 2.5 mol% MC component ($PG_{97.5}$-$MC_{2.5}$) to 30 mol% MC component (PG_{70}-MC_{30}) show rapid nucleation of amphibole. Synthesis attempts on the $PG_{97.5}$-$MC_{2.5}$ composition produced the best yields of amphibole with only traces of minor accessory clinopyroxene (discernible only under the SEM). Bulk compositions richer in the MC component showed poorer yields, with increasing amounts of accessory clinopyroxene, plagioclase, and either forsterite or enstatite, depending on the degree of silica undersaturation in the ambient fluid. Retreatments of the synthesis products made from the MC-rich bulk compositions tended to give *poorer* yields of amphibole and greater amounts of coexisting phases. This suggests that the initially formed amphibole is metastably enriched in the MC component, perhaps owing to its rapid nucleation, and then shifts toward pargasite with retreatment. This behavior was best seen for the experiments performed on the bulk composition $PG_{85}MC_{15}$ where the compositional shift was detected both by a change in the aggregate chemical composition of the grains with the electron microprobe (as seen in Fig. 4), as well as by an unusually large initial splitting of the 151 and $\bar{3}31$ XRD peaks (as discussed previously).

Amphibole synthesis attempts along the PG-TR join

To determine the extent of pargasite substitution in tremolite, the pargasite (PG)-tremolite (TR) join was studied hydrothermally in the range of 750–950 °C and 3–6 kbar using a series of oxide mixtures prepared along the join at an interval of 10 mol% PG. The results of these experiments are listed in Table 2. All of the compositions produced rapid nucleation of amphibole but none of the syntheses showed 100% yield, with variable amounts of clinopyroxene as the dominant additional phase. Minor amounts of plagioclase or gehlenite, and enstatite

TABLE 2. Syntheses along the PG-MC and PG-TR compositional joins

Nominal composition	Code	*T* (°C)	*P* (kbar)	*t* (h)	Products and comments*
The join PG-MC					
PG_{100}	PG-18	950(5)	4.0(1)	85	amph (~98%) + [plag]
	PG-69A	950(5)	3.0(1)	156	amph (~98%) + [plag]
	PG-164	800(5)	5.0(1)	160	amph (~30%) + cpx + plag + en
	PG-167A†	930(5)	3.4(1)	178	amph (~50%) + cpx + plag + geh
	PG-169A†	950(5)	3.0(1)	133	amph (~95%) + geh
	PG-170A	950(5)	3.0(1)	182	amph (~98%) + [geh]
$PG_{97.5}MC_{2.5}$	PC-70A	930(5)	3.0(1)	131	amph (~99%)
(=PCa)	PC-83	930(5)	3.0(1)	82	amph (~99%)
	PC-87†	700(5)	2.0(1)	450	amph (~99%) + [cpx]
	PC-111	900(5)	4.0(1)	191	amph (~99%) + [plag]
	PC-170B	950(5)	3.0(1)	182	amph (~90%) + plag + fo +[cpx]
	PARG 11-4	897(4)	1.01(5)	74	amph (~95%) + [cpx]
	PARG 11-7	895(16)	1.32(5)	188	amph (98%) + [plag] + [cpx]
$PG_{95}MC_5$	PC-70B	930(5)	3.0(1)	131	amph (~98%) + [plag] + [cpx] + [fo]
(=PCb)	PC-170C	950(5)	3.0(1)	182	amph (~95%) + geh + fo + [cpx]
$PG_{92.5}MC_{7.5}$	PC-70C	930(5)	3.0(1)	131	amph (~98%) + [plag] + [fo] + [cpx]
	PC-173E†	950(5)	3.3(1)	126	amph (~97%) + fo
$PG_{90}MC_{10}$	PC-43A	850(5)	6.0(1)	340	amph (~95%) + en
	PC-68D	950(5)	3.0(1)	72	amph (~95%) + plag + fo + [cpx]?
	PC-173A†	950(5)	3.3(1)	126	amph (~95%) + fo
$PG_{85}MC_{15}$	PC-69B	950(5)	3.0(1)	156	amph (~95%) + fo
	PC-70F	930(5)	3.0(1)	131	amph (~90%) + plag + fo + [cpx]
	PC-173B†	950(5)	3.3(1)	126	amph (~90%) + fo + plag + [cpx]
$PG_{80}MC_{20}$	PC-69C	950(5)	3.0(1)	156	amph (~80%) + plag + fo + cpx
	PC-173D†	950(5)	3.3(1)	126	amph (~80%) + fo + plag + cpx
$PG_{70}MC_{30}$	PC-69D	950(5)	3.0(1)	156	amph (~80%) + plag + fo + cpx
The join PG-TR					
$PG_{90}TR_{10}$	PT-155A	900(5)	5.0(1)	264	amph (~70%) + geh + cpx + en
	PT-167B	930(5)	3.5(1)	178	amph (~50%) + cpx + geh + en
	PT-169B†	950(5)	3.0(1)	133	amph (~90%) + geh + cpx + fo
	PT-170D	950(5)	3.0(1)	178	amph (~90%) + geh + cpx + fo
$PG_{80}TR_{20}$	PT-167C	930(5)	3.5(1)	178	amph (~95%) + cpx
	PT-170E	950(5)	3.0(1)	182	amph (~95%) + cpx
	PARG 15-1	962(3)	2.02(5)	162	amph (~80%) + cpx + plag + fo
	PARG 15-2†	965(6)	1.85(5)	163	amph (~75%), slight increase in cpx + plag + fo
	PARG 15-3	881(17)	1.08(5)	433	amph (92%) + cpx + [fo], 0.5m NaOH solution
$PG_{70}TR_{30}$	PT-121A	800(5)	5.0(1)	238	amph (~95%) + cpx
	PT-128D	850(5)	5.0(1)	328	amph (~70%) + cpx + en + [plag?]
	PT-164C†	800(5)	5.0(1)	160	amph (~80%) + cpx + en + [plag?]
	PT-167D†	930(5)	3.5(1)	178	amph (~95%) + cpx
	PT-170F	950(5)	3.0(1)	182	amph (~95%) + cpx
$PG_{60}TR_{40}$	PT-166B	800(5)	5.0(1)	140	amph (~70%) + cpx + en + [plag?]
	PT-168	875(5)	5.0(1)	140	amph (~90%) + cpx
$PG_{50}TR_{50}$	PT-44	750(5)	6.0(1)	204	amph (~85%) + cpx + en + plag
	PT-45†	750(5)	6.0(1)	261	amph (~90%) + cpx
	PT-128G	850(5)	5.0(1)	328	amph (~80%) + cpx + en + [plag?]
	PT-164D†	800(5)	5.0(1)	160	amph (~90%) + cpx
	PT-168B†	875(5)	5.0(1)	140	amph (~90%) + cpx
$PG_{40}TR_{60}$	PT-166C	800(5)	5.0(1)	140	amph (~70%) + cpx + plag + en
	PT-168C†	875(5)	5.0(1)	140	amph (~90%) + cpx
$PG_{30}TR_{70}$	PT-104	850(5)	5.6(1)	287	amph (~90%) + cpx + qtz
	PT-106A	800(5)	6.0(1)	162	amph (~90%) + cpx + qtz
	PT-115A	800(5)	5.0(1)	333	amph (~90%) + cpx + qtz
	PT-164E†	800(5)	5.0(1)	160	amph (~90%) + cpx + qtz
	PT-168D†	875(5)	5.0(1)	140	amph (~90%) + cpx + qtz
$PG_{20}TR_{80}$	PT-166D	800(5)	5.0(1)	140	amph (~85%) + cpx + qtz
	PT-168E†	875(5)	5.0(1)	140	amph (~85%) + cpx + qtz
TR_{100}	TR-114q	800(5)	5.1(1)	314	amph (~80%) + cpx + qtz

Note: Uncertainty in last digit shown in parentheses; q after code number indicates the addition of about 5 wt% quartz to the starting mixture.
* Phases listed in order of abundance; amphibole abundance (wt%) indicated in parentheses; ~ = abundances estimated via relative peak heights with uncertainties of ±10 wt%, otherwise abundances are via Rietveld refinement with uncertainties of ±2 wt%; [] = trace phase (<2 wt%). Abbreviations: amph = amphibole; cpx = diopsidic clinopyroxene; en = enstatite; fo = forsterite; geh = gehlenite; neph = nepheline; plag = plagioclase; qtz = quartz.
† Retreatment of the synthesis products from the immediately preceeding experiment in the table.

or forsterite were also observed, the particular mineral assemblage depending on the degree of silica undersaturation of the ambient fluid as controlled by the amphibole composition. Retreatment of the run products, as well as changing the physical conditions of synthesis consistently resulted in the production of amphibole + clinopyroxene. Earlier studies (e.g., Jenkins 1987; Graham et al. 1989; Pawley et al. 1993) on the synthesis of tremolite have indicated similar results. Due to the presence of clinopyroxene as the major accessory phase, the composition of the amphibole must shift away from the TR-PG bulk composition join along a straight line joining diopside and the starting composition. This effect is shown on the chemographic diagram in Figure 5 by a straight-line reaction relation: x (amphibole-2) + y (clinopyroxene) = z (amphibole-1). Note that a

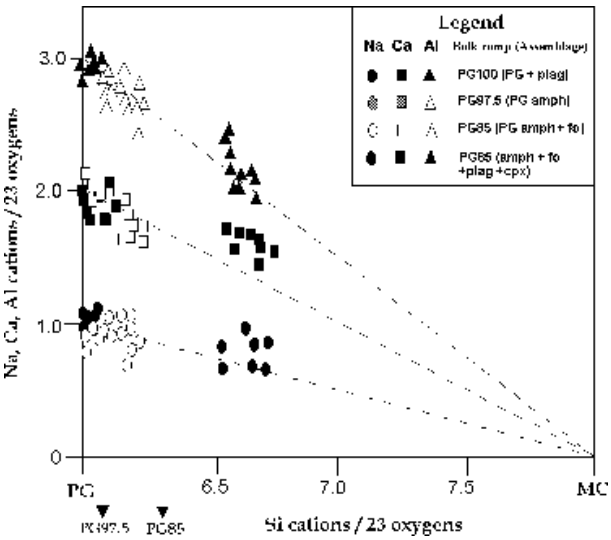

FIGURE 4. Variations in Na, Ca, and Al with Si content (apfu) for amphiboles formed along the PG-MC join. The Si content of the $PG_{97.5}MC_{2.5}$ and of the $PG_{85}MC_{15}$ bulk compositions are shown by vertical dashed lines. The solid symbols show the compositions of amphiboles made from the $PG_{85}MC_{15}$ bulk composition where only forsterite (fo) coexists, whereas the open symbols show the compositions of the amphiboles made from the same bulk composition where forsterite, plagioclase (plag), and clinopyroxene (cpx) are all present. Note the clustering of amphibole compositions about $PG_{97.5}MC_{2.5}$.

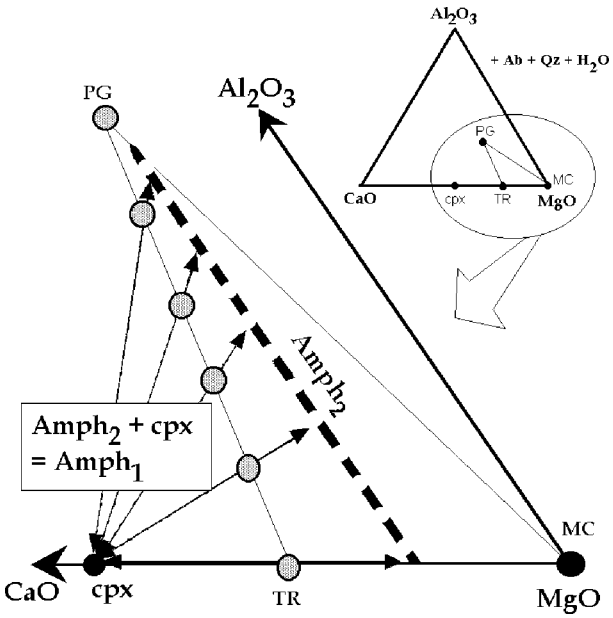

FIGURE 5. Projection from albite (Ab) + quartz (qz) and water into the ternary subsystem CaO-MgO-Al_2O_3 schematically showing the chemographic relationships for amphiboles synthesized along the PG-TR join. The shaded circles indicate specific bulk compositions ($Amph_1$) along the PG-TR join whereas the dashed arrows indicate shifts in the composition of amphibole ($Amph_2$) required by the coexistance of clinopyroxene (cpx). TR-rich compositions appear to show a greater shift towards MC enrichment than the PG-rich compositions.

similar shift in amphibole compositions away from the TR-PG join is required even if plagioclase or gehlenite are present, though not necessarily in a straight line from clinopyroxene. With increasing PG content the amount of clinopyroxene decreases, implying that the compositional shift of the synthesized amphibole becomes smaller. Finally, at PG_{100}, the amphibole composition is nearly stoichiometric pargasite. The microprobe analyses of the run products along the PG-TR join shown in Figure 6 confirm this behavior by showing compositional offset from the PG-TR join into the PG-TR-MC ternary. For these analyses, the mol% PG is calculated from the total Al [Al(T)] cations and the mol% MC is calculated from the Mg content in the M4 site. These results suggest the presence of a possible solid-solution region offset toward MC-component. This contradicts the earlier studies of Oba (1980, 1990), who reported observing pure amphibole yields along most of the tremolite-pargasite join under similar conditions of synthesis.

In general there is rapid nucleation and production of amphibole along the PG-TR join; however, with increasing pargasite content, it was necessary to increase the temperature of synthesis to maintain a similar reaction rate or yield. An exception to the rapid reaction rate was the composition PG_{90}, for which only an incomplete reaction was observed (Fig. 7). In addition, the $\Delta 2\theta$ [(151)-($\bar{3}$31)] variable was determined to be greater than that for pure pargasite. With further treatment of the reaction products, this anomalous $\Delta 2\theta$ [(151)-($\bar{3}$31)] value decreased to a value comparable to that of pargasite. Routine analytical techniques used in this study did not succeed in discriminating between the composition of this precursor amphibole and that of a "normal" amphibole formed after its retreatment. The origin of the poor yield of the synthesis reaction for this pargasite-rich amphibole has not been investigated in detail in this study; however, a detailed study of a pargasite-rich amphibole (approximately $PG_{80}TR_{20}$) within the TR-PG-MC ternary displaying similar poor yields is described below.

Syntheses in the TR-PG-MC ternary system

The main results of our study of the TR-PG join are that: (1) incomplete yields of amphibole were found along the entire join with clinopyroxene the dominant coexisting phase; (2) the yield of amphibole is lower for bulk compositions in the vicinity of $PG_{90}TR_{10}$; and (3) there is evidence for a small degree (~ 2.5 mol%) of Mg substitution for Ca in the M4 site of pargasitic amphibole, similar to the substitution of Mg for Ca in tremolitic amphibole that is supported most recently by the work of Zimmermann et al. (1996). With this in mind, we investigated bulk compositions primarily within the ternary system TR-PG-MC along three joins, as shown in Figure 1: (a) $PG_{97.5}MC_{2.5}$-$TR_{90}MC_{10}$ (PCa-TCa), (b) $PG_{95}MC_5$-$TR_{85}MC_{15}$ (PCb-TCb), (c) $PG_{95}MC_5$-$TR_{80}MC_{20}$ (PCb-TCc). These joins were studied to discern the extent of MC solid-solution into amphibole and the sluggish kinetics near the pargasite apex.

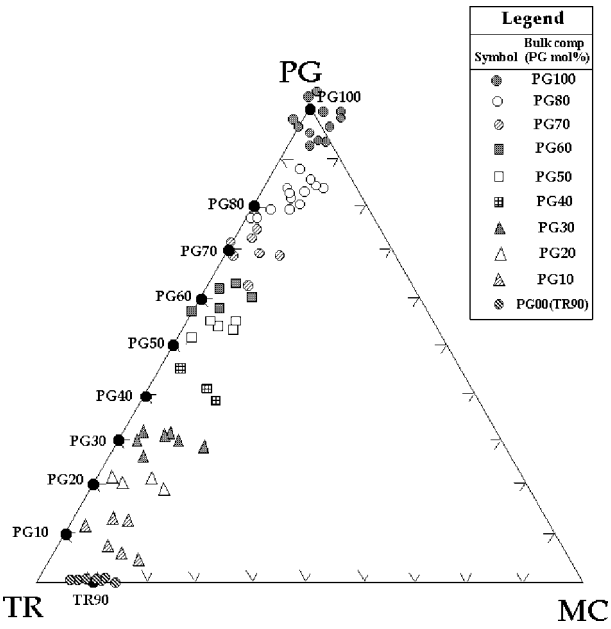

FIGURE 6. Electron microprobe analyses of amphiboles formed from bulk compositions at 10 mol% increments along the PG-TR join (solid circles). Legend shows the bulk compositions from which the various amphiboles were formed. Notice the clustering of the analyses toward MC enrichment, i.e., within the body of the ternary diagram.

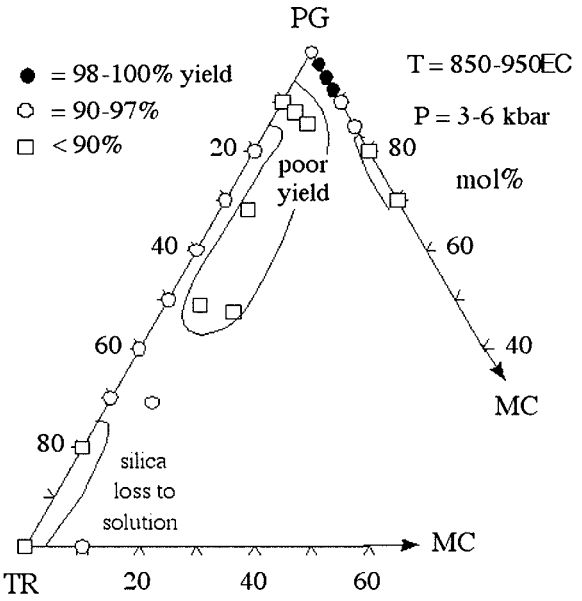

FIGURE 7. Amphibole synthesis results from experiments performed in the range of 850–950 °C and 3–6 kbar shown on a portion of the TR-PG-MC ternary diagram. Shaded circle = highest-yields (98–100 wt%); open circle = next highest yields (90–97%); square = lowest yields (<90%). Areas of poor yield are indicated as well as the region where strong loss of silica to solution occurs.

The join $PG_{97.5}MC_{2.5}$-$TR_{90}MC_{10}$ (PCa-TCa). The experimental results of syntheses along this join are listed in the first half of Table 3. Syntheses performed along this join at the same pressures and temperatures as the TR-PG join, i.e., 3–6 kbar and 850–950 °C, produced relatively poor yields (40–60 wt%) except for the TR-rich bulk compositions (>TR_{60}). This field of poor amphibole yield is shown on Figure 7 along with the synthesis results obtained in this *P-T* range for all other joins studied here. There is also a field of poor yield near the TR apex related to the loss of silica to solution at these high *P-T* conditions. Dropping the pressure to 1–1.5 kbar and keeping the temperature in the range 875–950 °C increased the yield markedly for PG-rich compositions. These temperatures are either above the thermal stability of tremolitic amphibole or too close to the breakdown boundary to allow good nucleation and growth; therefore, optimal yields for the tremolite-rich portion of the join were obtained at about 800 °C and 4–5 kbar.

Very good yields (97–98 wt%) of pargasitic amphibole were obtained at these lower-pressure (1–1.5 kbar) conditions for bulk compositions PARG 11 and PARG 16 but not for PARG 13. This latter bulk composition is similar to the problematic composition ($PG_{90}TR_{10}$) encountered along the TR-PG join and considerable effort was invested in this bulk composition to see if the incomplete yield was kinetic or compositional in nature. In all cases where PARG 13 was treated in water, the yields consisted of about 75 wt% amphibole with the remainder being plagioclase (~An_{67} based on electron microprobe analysis), diopsidic clinopyroxene, and forsterite. Reaction rate does not appear to be the limiting factor, because repeated treatments of the same mixture produced no improvement in the yield of amphibole. A portion of the PARG 13 oxide starting mixture was melted to a clear glass at 1450 °C (PARG 13–34) and hydrothermally treated to see if the nucleation of non-amphibole phases could be suppressed, but with no success.

The variable that produced the greatest improvement in the yield was the addition of NaOH solution, suggesting that incomplete amphibole yields were linked with the loss of Na to the ambient fluid. Many experiments (28) were performed on the bulk composition PARG 13 using NaOH solutions varying in molality from 0.25 to 4.5 *m* to test the Na-loss hypothesis. The results of these experiments are listed in Table 3. Optimal yields of amphibole (95 wt%) were obtained using 0.25–0.5 *m* NaOH solutions, whereas the more-concentrated solutions promoted the nucleation of other phases (nepheline, gehlenite, layer silicate) without a noticeable increase in the amphibole yield. The results of these lower NaOH concentration experiments are listed in Table 3. Increasing silica in the ambient solution, by the addition of quartz to the starting mixture (PARG 13-36, 13-38), produced a relative increase in plagioclase whereas increasing the forsterite in the system (PARG 13-40) caused a decrease in plagioclase. These observations are consistent with the reaction:

TABLE 3. Conditions and products of synthesis for selected experiments within the ternary system TR-PG-MC

Nominal composition	Code	*T* (°C)	*P* (kbar)	*t* (h)	fluid (wt%)	Products and comments*
The join PCa-TCa						
$PCa_{90}TCa_{10}$	PTC-128B	800(5)	5.0(1)	328	H_2O (~20%)	amph (~40%) + cpx + fo + plag
	PTC-160C†	900(5)	2.0(1)	91	H_2O (~20%)	amph (~50%) + geh + cpx + fo
	PTC-161B	850(5)	5.0(1)	427	H_2O (~20%)	amph (~55%) + cpx + plag + en
	PTC-163F†	850(5)	5.5(1)	188	H_2O (~20%)	amph (~60%) + cpx + plag + en
	PTC-163A	850(5)	5.5(1)	188	H_2O (~20%)	amph (~50%) + cpx + en + geh
	PTC-165C†	850(5)	5.0(1)	186	H_2O (~20%)	amph (~50%) + cpx + plag + fo
	PTC-167F†	950(5)	3.0(1)	356	H_2O (~20%)	amph (~70%) + cpx + en + [geh]
"$PCa_{80}TCa_{20}$"	PARG 14-1	962(3)	2.02(5)	162	H_2O (18%)	amph (~85%) + cpx + plag + fo
($PG_{79}TR_{19}MC_2$)	PARG 14-2†	965(6)	1.85(5)	163	H_2O (19%)	amph (~75%), increase in cpx + plag + fo
	PARG 14-3†	883(15)	1.16(5)	507	0.25m NaOH (29%)	amph (93%), decrease in cpx + plag, no fo
$PCa_{80}TCa_{20}$	PARG 13-1	962(3)	2.02(5)	162	H_2O (9%)	amph (~80%) + cpx + plag + fo
	PARG 13-2†	965(6)	1.85(5)	163	H_2O (20%)	amph (~75%), increase in cpx + plag + fo
	PARG 13-13	934(5)	1.90(7)	263	H_2O (8%)	amph (~80%)+ cpx + plag + fo
	PARG 13-15†	935(5)	2.00(5)	264	H_2O (8%)	amph (~85%), possible decrease in cpx + plag + fo
	PARG 13-17†	933(18)	1.98(8)	384	H_2O (9%)	no change from PARG 13-15
	PARG 13-19	890(10)	1.95(5)	378	H_2O (20%)	amph (~80%) + plag + cpx + [fo]?
	PARG 13-24	886(13)	1.04(5)	222	H_2O (22%)	amph (~65%) + cpx + plag + fo
	PARG 13-25†	883(19)	1.06(5)	168	H_2O (24%)	no change from PARG 13-24
	PARG 13-26†	897(4)	1.01(5)	74	1.0m NaOH (26%)	amph (~90%), decrease in cpx + fo, [neph]
	PARG 13-34§	895(13)	1.05(5)	198	H_2O (23%)	amph (~60%), more plag + cpx + fo than from oxides
	PARG 13-44	880(40)	1.15(5)	411	H_2O (21%)	amph (74%) + cpx + plag + fo
	PARG 13-29	889(12)	1.01(5)	118	0.5m NaOH (24%)	amph (~80%) + plag + cpx + fo
	PARG 13-31†	892(10)	0.97(5)	46	0.5m NaOH (25%)	amph (~85%) + cpx + [neph]
	PARG 13-36‡	893(4)	1.10(5)	453	0.5m NaOH (25%)	amph (~80%) + plag + cpx + [fo]
	PARG 13-37†	893(4)	1.03(5)	335	0.5m NaOH (26%)	no change from PARG 13-36
	PARG 13-38†‡	890(6)	1.11(5)	504	0.5m NaOH (25%)	amph (~85%), increase in plag, no change in cpx, no fo
	PARG 13-39	875(21)	1.14(5)	244	0.25m NaOH (38%)	amph (~80%) + cpx + [plag]
	PARG 13-40‖	875(21)	1.14(5)	244	0.5m NaOH (28%)	amph (~80%) + cpx + fo
	PARG 13-41	883(7)	1.16(5)	167	0.25m NaOH (21%)	amph (~75%) + cpx + plag + fo
	PARG 13-42†	894(12)	1.29(5)	168	0.25m NaOH (24%)	amph (95%), decrease in cpx + [plag], no fo
	PARG 13-43†	882(18)	1.37(5)	98	0.5m NaOH (23%)	no change from PARG 13-42
$PCa_{70}TCa_{30}$	PTC-163B	850(5)	5.5(1)	188	H_2O (~20%)	amph (~40%) + cpx + plag + en
	PTC-165D†	850(5)	5.0(1)	186	H_2O (~20%)	amph (~60%) + cpx + plag + fo
	PTC-167G†	930(5)	3.0(1)	356	H_2O (~20%)	amph (~60%) + cpx + plag + en
$PCa_{60}TCa_{40}$	PARG 16-5	798(8)	4.00(5)	306	H_2O (32%)	amph (97%) + cpx
	PARG 16-6†	800(13)	3.97(20)	189	H_2O (31%)	no change from PARG 16-5
	PARG 16-8	790(5)	1.00(5)	2116	H_2O (18%)	amph (70%) + cpx + plag + fo
$PCa_{50}TCa_{50}$	PTC-163C	850(5)	5.5(1)	188	H_2O (~20%)	amph (~50%) + cpx + en
	PTC-165E†	850(5)	5.0(1)	186	H_2O (~20%)	amph (~70%) + cpx + en
	PTC-167H†	930(5)	3.0(1)	356	H_2O (~20%)	amph (~75%) + cpx + en
$PCa_{40}TCa_{60}$	PARG 17-1	798(3)	3.90(15)	118	H_2O (25%)	amph (~80%) + cpx
	PARG 17-2†	800(9)	4.02(5)	480	H_2O (31%)	amph (~85%), slight decrease in cpx
	PARG 17-3‡	802(6)	4.06(5)	337	H_2O (23%)	amph (~100%)
	PARG 17-4‡	803(13)	3.98(5)	668	H_2O (20%)	amph (96%)+ plag
$PCa_{30}TCa_{70}$	PTC-106B	800(5)	6.0(1)	162	H_2O (~20%)	amph (~99%) + [plag]
	PTC-110A†	800(5)	5.0(1)	187	H_2O (~20%)	amph (~99%) + [plag]
	PTC-165F‡	850(5)	5.0(1)	186	H_2O (~20%)	amph (~95%) + cpx + en + plag
$PCa_{20}TCa_{80}$	PARG 18-3‡	802(14)	4.00(5)	768	H_2O (30%)	amph (100%)
TCa_{100}	TC-31	850(5)	6.0(1)	166	H_2O (~20%)	amph (~60%) + cpx + en
	TC-32†‡	850(5)	6.0(1)	63	H_2O (~20%)	amph (~95%) + qtz
	TC-50‡	850(5)	6.0(1)	219	H_2O (~20%)	amph (~95%) + qtz
	TREM 23-13‡	801(5)	4.52(5)	458	H_2O (31%)	amph (94%) + cpx + quartz
The join PCb-TCb						
$PCb_{80}TCb_{20}$	PARG 19-12	882(11)	1.18(5)	327	H_2O (27%)	amph (76%) + plag + for + cpx
	PARG 19-6	873(18)	0.97(5)	341	0.25m NaOH (30%)	amph (~80%) + plag + cpx + fo
	PARG 19-7†	847(40)	1.12(5)	141	H_2O (28%)	little change from PARG 19-6
	PARG 19-8†	883(15)	1.16(5)	507	0.25m NaOH (30%)	amph (~95%)+ [plag]
	PARG 19-9	887(14)	1.16(5)	355	0.5m NaOH (23%)	amph (~90%) + plag + cpx + fo
	PARG 19-11†	890(5)	1.15(7)	524	0.25m NaOH (30%)	amph (99%) + [plag]
$PCb_{60}TCb_{40}$	PARG 20-2	800(16)	4.00(5)	456	H_2O (29%)	amph (98%) + [cpx]
$PCb_{40}TCb_{60}$	PARG 21-1	797(4)	3.98(5)	213	H_2O (31%)	amph (~99%) + [cpx]?
	PARG 21-2‡	795(17)	4.00(5)	264	H_2O (30%)	amph (99%) + [plag]
The join PCb-TCc						
$PCb_{90}TCc_{10}$	PTC-125E	800(5)	5.0(1)	288	H_2O (~20%)	amph (~40%) + geh + cpx + en
	PTC-155C	900(5)	5.0(1)	264	H_2O (~20%)	amph (~30%) + cpx + geh + en
$PCb_{70}TCc_{30}$	PTC-125C	800(5)	5.0(1)	288	H_2O (~20%)	amph (~30%) + cpx + en
$PCb_{50}TCc_{50}$	PTC-163E	850(5)	5.5(1)	188	H_2O (~20%)	amph (~60%) + cpx + en
$PCb_{30}TCc_{70}$	PTC-113‡	800(5)	6.0(1)	148	H_2O (~20%)	amph (~90%) + cpx + plag + [en]

Note: Uncertainty in last digit shown in parentheses.

* Phases listed in order of abundance; amphibole abundance (wt%) indicated in parentheses; ~ = abundances estimated via relative peak heights with uncertainties of ±10 wt%, otherwise abundances are via Rietveld refinement with uncertainties of ±2 wt%; [] = trace phase (<2 wt%). Abbreviations: same as in Table 2.

† This is a retreatment of the synthesis products from the immediately preceding experiment in the table. If a NaOH solution was used in the previous experiment, the sample was rinsed in water to remove any residual NaOH prior to retreatment.

‡ Starting oxide mixture was enriched with 3–5 wt% synthetic quartz prior to treatment.

§ Starting oxide mixture was vitrified at 1450°C for 45 minutes to a clear glass and finely powdered prior to treatment.

‖ Starting oxide mixture was enriched with 5 wt% synthetic forsterite prior to treatment.

TABLE 4. Electron microprobe analyses of selected amphiboles synthesized in this study

Sample code	PARG 11-4	PARG 11-7	PARG 15-2	PARG 15-3	PARG 14-3	PARG 13-39	PARG 13-43	PARG 13-44	PARG 19-8
wt% oxide	n = 13	10*	13*	7	7	8	13	13*	17
SiO_2	42.9(18)	40.4(25)	41.6(23)	45.2(25)	46.5(14)	44.6(21)	43.0(11)	41.1(17)	45.8(31)
Al_2O_3	18.1(16)	16.1(10)	11.4(7)	14.4(20)	14.1(5)	15.5(15)	11.2(8)	13.1(8)	13.0(12)
MgO	19.9(11)	19.5(10)	19.3(14)	20.4(16)	21.1(7)	20.2(9)	19.5(5)	19.3(10)	20.9(13)
CaO	12.7(7)	12.3(6)	11.0(3)	12.5(8)	12.6(6)	12.4(4)	11.0(4)	10.9(4)	12.2(4)
Na_2O	3.69(21)	3.27(39)	3.03(34)	3.56(36)	3.57(12)	3.60(14)	3.44(26)	3.17(29)	3.41(19)
Total	97.3(36)	91.5(37)	86.4(48	96.1(45)	97.8(21)	96.3(32)	88.0(14)	87.5(36)	95.3(50)
Formula proportions of cations based on 23 oxygen atoms									
Si	6.00(13)	6.00(22)	6.52(5)	6.38(16)	6.43(7)	6.27(16)	6.60(12)	6.35(7)	6.49(15)
Al(T)	2.98(23)	2.82(17)	2.11(5)	2.39(34)	2.29(9)	2.57(25)	2.02(16)	2.38(12)	2.18(20)
$^{[IV]}$Al(=8-Si)	2.00(12)	2.00(22)	1.48(5)	1.62(16)	1.57(7)	1.73(15)	1.40(11)	1.65(7)	1.51(15)
$^{[VI]}$Al	0.98(11)	0.82(11)	0.63(4)	0.77(18)	0.72(4)	0.84(11)	0.62(8)	0.73(7)	0.67(8)
Mg	4.14(16)	4.32(14)	4.49(9)	4.29(20)	4.36(6)	4.24(10)	4.45(9)	4.44(7)	4.42(9)
$^{[VI]}$Mg(=5-$^{[6]}$Al)	4.02(11)	4.18(11)	4.37(4)	4.23(18)	4.28(4)	4.16(11)	4.38(8)	4.27(7)	4.33(8)
$^{[M4]}$Mg	0.12(7)	0.14(5)	0.12(8)	0.06(3)	0.08(4)	0.08(2)	0.07(6)	0.17(6)	0.09(4)
Ca	1.89(6)	1.96(8)	1.85(8)	1.89(7)	1.87(5)	1.87(3)	1.81(6)	1.81(5)	1.86(5)
Na	1.00(5)	0.94(10)	0.92(7)	0.97(9)	0.96(2)	0.98(2)	1.02(8)	0.95(7)	0.94(3)
Total	16.01(6)	16.06(19)	15.89(7)	15.90(5)	15.90(3)	15.94(5)	15.90(10)	15.93(6)	15.89(7)

Note: Uncertainties (1s) in last decimal place shown in parentheses. Tabulated data are averages of (n) individual analyses. nd = not determined.
* EDS analysis; all others via WDS.

$$0.98\ CaMgSi_2O_6 + 1.66\ Mg_2SiO_4 +$$
clinopyroxene olivine

$$1.40\ Na_{0.33}Ca_{0.67}Al_{1.67}Si_{2.33}O_8 + 0.84\ H_2O + 0.32\ NaOH_{aq} =$$
plagioclase (An_{67})

$$Na_{0.78}Ca_{1.92}Mg_{4.30}Al_{2.34}Si_{6.44}O_{22}(OH)_2 + 0.46\ SiO_{2,\,aq} \quad (1)$$
amphibole

assuming the amphibole has the composition of PARG 13. The relatively poor yields observed for bulk compositions near 80–90 mol% PG may be caused by a marked deviation in the partitioning of Na between the amphibole and the ambient solution, possibly related to some optimal complexing of Na and silica in solution for these bulk compositions. Alternatively, the amphibole formed in this composition range may simply require more Na than the rest of the join (see below).

The tremolitic portion of this join (PARG 17, 18, TREM 23) produced nearly complete yields of amphibole, particularly when 3–5 wt% additional quartz was added to offset the loss of silica to the ambient solution (Jenkins 1987). As with the TR-PG join, diopsidic clinopyroxene was generally present as the main extraneous phase, especially for bulk compositions near the middle of this join, suggesting that these amphiboles exhibit further enrichment in Mg.

The join $PG_{95}MC_5$-$TR_{85}MC_{15}$ (PCb-TCb). Three composi-

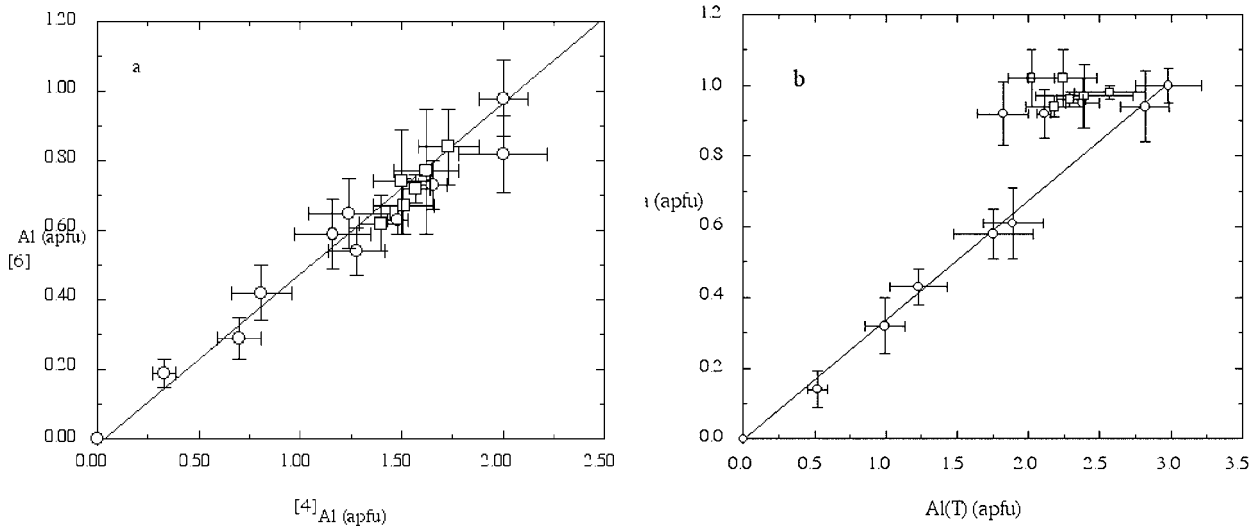

FIGURE 8. (**a**) Variation in $^{[VI]}$Al with $^{[IV]}$Al (apfu) of amphiboles synthesized within the TR-PG-MC ternary system based on the electron microprobe analyses listed in Table 4. The solid line is the variation one would predict for amphiboles formed along the $TR_{90}MC_{10}$-$Pg_{97.5}MC_{2.5}$ join. (**b**) Variation in Na vs. Al(T) (total Al) with the solid line showing the expected variation. Squares represent mixtures treated in a 0.25 *m* NaOH solution.

Table 4 —*Extended.*

Sample code	PARG 19-11	PARG 19-12	PARG 16-6	PARG 20-2	PARG 17-4	PARG 21-1	PARG 18-3	TREM 23-13
wt% oxide	n =13	12*	13*	17*	18*	10*	21*	8*
SiO_2	44.1(12)	43.9(25)	48.8(32)	47.9(27)	49.2(50)	47.4(14)	53.4(62)	49.5(86)
Al_2O_3	12.9(15)	10.1(9)	11.5(11)	10.4(17)	5.6(10)	6.9(13)	3.05(39)	0.01(3)
MgO	20.1(9)	20.2(13)	22.0(8)	21.4(13)	21.9(25)	21.6(9)	23.2(26)	21.5(41)
CaO	10.8(3)	10.7(4)	12.0(5)	12.0(5)	11.9(10)	10.3(11)	12.1(14)	10.4(13)
Na_2O	3.56(28)	3.09(39)	2.28(36)	2.10(27)	1.13(33)	1.48(22)	0.51(18)	nd
Total	91.6(21)	88.4(41)	96.7(31)	93.9(41)	89.8(90)	87.6(36)	92(10)	81(13)
			Formula proportions of cations based on 23 oxygen atoms					
Si	6.50(14)	6.72(14)	6.76(20)	6.84(20)	7.30(11)	7.19(15)	7.67(6)	8.00(4)
Al(T)	2.24(24)	1.82(18)	1.89(21)	1.75(28)	0.99(14)	1.23(20)	0.52(7)	0.003(5)
$^{[IV]}$Al(=8-Si)	1.50(14)	1.28(14)	1.24(20)	1.16(19)	0.70(11)	0.81(15)	0.33(6)	0.0
$^{[VI]}$Al	0.74(15)	0.54(7)	0.65(10)	0.59(10)	0.29(6)	0.42(8)	0.19(4)	0.0
Mg	4.41(18)	4.61(10)	4.54(12)	4.55(12)	4.84(13)	4.89(10)	4.95(9)	5.17(14)
$^{[VI]}$Mg(=5-$^{[6]}$Al)	4.26(15)	4.46(7)	4.35(10)	4.41(10)	4.71(6)	4.58(8)	4.81(4)	5.00
$^{[M4]}$Mg	0.15(7)	0.15(5)	0.19(6)	0.14(6)	0.13(11)	0.31(14)	0.14(8)	0.17(14)
Ca	1.71(6)	1.75(7)	1.79(9)	1.84(6)	1.90(12)	1.67(16)	1.86(8)	1.82(20)
Na	1.02(8)	0.92(9)	0.61(10)	0.58(7)	0.32(8)	0.43(5)	0.14(5)	nd
Total	15.88(11)	15.83(11)	15.60(17)	15.58(9)	15.36(9)	15.41(9)	15.14(5)	14.99(4)

tions were investigated along this join (PARG 19, 20, 21; Fig. 1). As with the PARG 13 bulk composition, a good yield of amphibole was obtained only for the PARG 19 bulk composition by using a 0.25m NaOH solution. The other two bulk compositions produced nearly complete yields of amphibole using only water (and minor additional quartz for PARG 21) with only traces of clinopyroxene discerned in the X-ray patterns. These compositions are deemed to be at or very near the Ca-rich limit of solid solution within the TR-PG-MC ternary system. No effort was made to define the Mg-rich limit of amphibole miscibility.

The join $PG_{95}MC_5$-$TR_{80}MC_{20}$ (PCb-TCc). Four compositions were studied along this join (Fig. 1, Table 3), which is shifted toward slightly higher MC content at the TR-rich end of the join compared to the PCb-TCb join discussed above. Experiments were performed in the range of 800–950 °C and 5–6 kbar, and the results of these experiments are listed in Table 3. All of the experiments indicated poor reaction and incomplete yields, with gehlenite, diopside, and enstatite as the accessory phases for the PG-rich compositions. The best yield was obtained for the most TR-rich composition studied (PCb_{30}). These experiments reinforce the observation that high pressure generally reduces the yield for PG- compared to TR-rich bulk compositions. Lower-pressure syntheses were not pursued along this join.

Compositions of amphiboles in the TR-PG-MC system

Electron microprobe analyses of individual amphibole crystals were obtained from selected syntheses within the TR-PG-MC ternary system, and are listed in Table 4. Despite the inherently large uncertainties associated with these fine-particle analyses, the data are broadly consistent with the 1:2 variation in $^{[VI]}$Al:$^{[IV]}$Al (Fig. 8a) and the 1:3 variation in Na/Al(T) (Fig. 8b), which one would expect for amphiboles close to the tremolite-pargasite join. These substitutions result from the "pargasite" substitution of ^{A}Na + $^{[VI]}$Al + $^{[IV]}$Al = $^{A}\square$ + $^{[VI]}$Mg + $^{[IV]}$Si, where $\square$ indicates a vacancy. The only exception to these trends appears in Figure 8b for the amphiboles with Al(T) ~2.4 apfu, which have a slightly higher than expected Na content. Although some of these amphiboles are from mixtures that were treated in NaOH solutions (squares), others (circles) are from mixtures treated in water. It appears that these samples have a genuine excess of Na over that expected from the pargasite substitution. This Na excess may simply be due to some minor substitution of Na for Ca on the M4 site, perhaps by the substitution $^{A}Na^{+1} + {}^{M4}Na^{+1} = {}^{A}\square + {}^{M4}Ca^{+2}$. This is supported by the observations that the amphibole chemistry shows no other deviation from the pargasite substitution, such as low Al(T) or high Si that would result from solid solution with richterite [$Na_2CaMg_5Si_8O_{22}(OH)_2$], and that there is a slight deficiency in the total Ca and Mg occupancy of the M4 site for amphiboles with Al(T) in the range of 2.0–2.4 (e.g., PARG 19-11, Table 4). Unfortunately this deficiency is about the same magnitude as the uncertainty in Ca and ^{M4}Mg precluding a clear proof of this hypothesis.

Rietveld structure refinements

Rietveld refinements were performed on relatively large-mass (150 mg) syntheses of selected bulk compositions that gave, in general, the highest amphibole yields. The pattern agreement statistics (R_P, R_{WP}, R_{exp}, GoF, and D) are listed in Table 5 along with the modal abundances (in wt%) and the agreement index (R_B) for each phase in the mixture. Owing to their minor abundance, the accessory phases were treated as having the same (fixed) composition in all of the mixtures. Structural information for plagioclase (An_{66}) was taken from Wenk et al. (1980), for diopside from Levien and Prewitt (1981), for forsterite from Liang and Hawthorne (1994), and for quartz from Lager et al. (1982). To correct partially for instrumental differences among all of these studies, the unit-cell dimensions of only these accessory phases were refined in a mixture containing the greatest abundance of these phases. The derived cell dimensions were then held constant in all other refinements and only the scale factors of the accessory phases were refined thereafter. The structure of amphibole was initiated using the structural data of Jenkins and Hawthorne (1995) for pargasitic amphibole and of Hawthorne and Grundy (1976) for tremolitic

amphibole. The refinement procedure that was followed here is described in detail in Jenkins and Hawthorne (1995). Briefly, the best results were obtained by first refining the zeropoint and unit-cell dimensions of the amphibole, holding all other parameters constant, and then by allowing the background, amphibole scale factor, peak half-width, preferred orientation, peak asymmetry, atomic coordinates, peak profile (pseudo-Voigt), overall isotropic displacement factor, and the scale factors of all other phases to be refined. Two sets of refinements were performed, one in which the composition of the amphibole was fixed to its nominal value, with the cations assigned to their "normal" sites (tetrahedral Al at T1, octahedral Al at M2 sites), and one in which the cation occupancy of Na on the A site and of Ca and Mg on the M4 sites were allowed to vary. The issue of Na on the M4 site was not pursued by Rietveld refinement because of complications from a three-atom refinement on this site. The unit-cell dimensions were the same in both cases. The unit-cell dimensions and refined cation occupancies are listed in Table 6. Refined atomic coordinates are reported in Table 7 for those bulk compositions producing nearly pure (>97 wt%) amphibole, i.e., those that are in the field of single-phase amphibole in the TR-PG-MC ternary system. Selected inter-atomic distances for these same amphiboles are listed in Table 8.

Rietveld refinements were also performed on selected compositions along the PG-TR join. Owing to the small volume of these samples, the refinement was limited to the range of 12–60° 2θ. Only the cell dimensions and cation contents are given for these samples in Table 6.

DISCUSSION

One of the main observations that we have made in this study is that amphiboles formed on the tremolite-pargasite join

TABLE 5. Agreement indices (%), whole-pattern parameters, modal analysis (wt%), and mineral agreement index (R_B) from Rietveld refinements

	Whole pattern					Minerals							
						amph		plag		cpx		other	
Sample code	R_P	R_{WP}	R_{EXP}	GoF	D	mode	R_B	mode	R_B	mode	R_B	mode	R_B
PARG 11-7	13.1	17.3	12.3	1.38	1.41	98(1)	6.2	1.4(2)	25.5	0.5(2)	18.9	–	
PARG 19-11	12.8	16.9	12.4	1.35	1.51	99(1)	7.2	1.0(2)	34.9	–		–	
PARG 19-12	12.5	16.5	13.2	1.24	1.35	76(1)	5.6	10.9(3)	9.6	5.6(2)	10.5	fo: 7.0(3)	8.4
PARG 13-43	12.8	17.4	13.1	1.31	1.36	95(1)	5.7	2.0(2)	27.9	3.0(2)	13.4	–	
PARG 13-44	11.9	16	13.3	1.19	1.46	74(1)	5.2	9.8(3)	11.0	9.8(3)	8.6	fo: 6.4(2)	8.9
PARG 16-6	12.3	16.1	12.3	1.29	1.21	97(1)	5.6	–		3.3(2)	12.9	–	
PARG 20-2	12.8	16.8	12.5	1.33	1.09	98(2)	5.6	–		1.8(2)	16.3	–	
PARG 17-4	12.9	17.1	12.6	1.34	0.87	96(2)	5.9	3.7(2)16.2		–		–	
PARG 21-2	11.8	15.9	12.3	1.27	1.26	99(1)	5.3	0.9(2)27.3		–		–	
PARG 18-3	10.7	14.7	12.2	1.19	1.46	100	4.4	–		–		–	
TREM 23-13	13.5	17.5	12.4	1.39	0.87	94(2)	7.1	–		3.2(3)	12	qtz: 3.1(1)	12

Note: $R_P = 100\Sigma|y_i - y_{ci}|/\Sigma|y_i|$, $R_{WP} = 100\{\Sigma w_i(y_i - y_{ci})^2/\Sigma w y_i^2\}^{1/2}$, $R_{EXP} = 100\{(N-P)/\Sigma w y_i^2\}^{1/2}$, GoF = Goodness-of-fit = R_{WP}/R_{EXP}, D = Durbin-Watson d statistic, $R_B = 100\{\Sigma|I_o - I_c|/\Sigma|I_o|$, where y_i and y_{ci} are the observed and calculated intensities at the ith step, $w_i = 1/y_i$, N = total number of steps, P = number of parameters being refined, I_o and I_c are the observed and calculated intensities for the Bragg reflections of each phase. Amphiboles assumed to have nominal compositions for these refinements. Phase abbreviations as in Table 2.

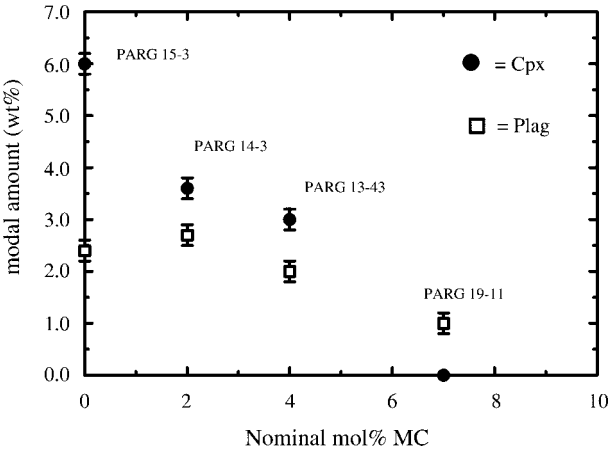

FIGURE 9. Modal abundance of clinopyroxene (Cpx, solid circles) and plagioclase (Plag, squares) produced from mixtures with approximately 80 mol% PG, plotted against the nominal mol% of MC in the bulk compositions.

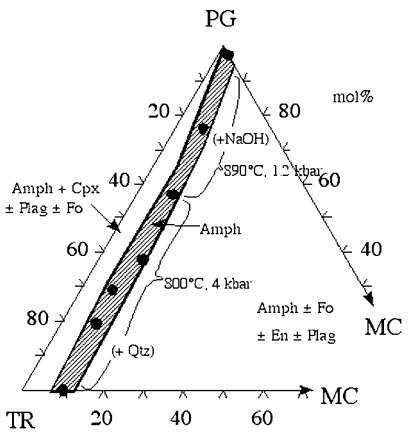

FIGURE 10. Polythermal (800–900 °C) and polybaric (1–4 kbar) projection of the field of complete amphibole miscibility (shaded region). Solid circles indicate compositions for which essentially complete yields were obtained. The approximate phase assemblages that are encountered are shown in the other areas.

TABLE 6. Unit-cell dimensions and refined cation occupancies (apfu) of Na on the A site and of Ca and Mg on the M4 site

Sample code	*a* (Å)	*b* (Å)	*c* (Å)	β (°)	*V* (Å³)	Na	Ca	Mg
PARG 11-7	9.8929(6)	17.944(1)	5.2804(3)	105.505(4)	903.25(9)	0.89(2)	1.62(6)	0.38(6)
PARG 19-11	9.9022(4)	17.9747(8)	5.2750(2)	105.384(3)	905.25(7)	0.85(2)	1.66(5)	0.34(5)
PARG 19-12	9.8880(6)	17.976(1)	5.2761(3)	105.320(5)	904.5(1)	0.88(2)	1.64(7)	0.36(7)
PARG 13-43	9.9007(5)	17.972(1)	5.2760(3)	105.393(4)	905.11(9)	0.88(2)	1.61(6)	0.39(6)
PARG 13-44	9.8963(6)	17.972(1)	5.2775(3)	105.389(5)	904.96(10)	0.89(3)	1.48(7)	0.51(7)
PARG 16-6	9.8548(7)	17.990(1)	5.2782(4)	105.137(4)	903.30(11)	0.59(2)	1.72(6)	0.28(6)
PARG 20-2	9.8466(8)	17.990(1)	5.2793(4)	105.099(5)	902.90(12)	0.56(2)	1.66(6)	0.34(6)
PARG 17-4	9.8279(7)	18.024(1)	5.2785(4)	104.867(5)	903.71(11)	0.35(2)	1.60(6)	0.40(6)
PARG 21-2	9.8184(6)	18.021(1)	5.2780(3)	104.829(4)	902.76(9)	0.28(2)	1.57(5)	0.43(5)
PARG 18-3	9.8160(5)	18.040(1)	5.2775(3)	104.741(3)	903.78(8)	0.15(2)	1.76(5)	0.24(5)
TREM 23-13	9.809(1)	18.054(2)	5.2763(6)	104.570(8)	904.32(17)	–*	1.77(8)	0.23(8)
PC-111†	9.8714(5)	17.934(1)	5.2768(3)	105.439(4)	900.46(8)	0.89(4)	1.62(7)	0.38(4)
PT-167C†	9.9245(6)	17.993(5)	5.2780(6)	105.520(5)	908.1(3)	0.72(4)	1.57(8)	0.43(5)
PT-167D†	9.8420(6)	17.968(7)	5.2775(6)	105.104(9)	901.0(4)	0.41(3)	1.68(6)	0.32(5)
PT-164E†	9.8180(6)	18.012(5)	5.2784(8)	105.052(8)	901.4(3)	0.23(4)	1.65(7)	0.35(6)

*Refinement with Na allowed on the A site caused strong distortions in the structure and was subsequently omitted.
† Small-volume samples, refined over a shorter angular range and to a lower precision than the samples in the first half of the table.

TABLE 7. Atomic coordinates from Rietveld refinement of amphiboles formed in the highest-yield syntheses

atom	PARG 11-7	PARG 19-11	PARG 20-2	PARG 21-2	PARG 18-3	TREM 23-13
O1						
x	0.1116(15)	0.1132(14)	0.1131(16)	0.1108(14)	0.1156(13)	0.1207(21)
y	0.0864(6)	0.0871(6)	0.0866(7)	0.0864(6)	0.0850(5)	0.0876(9)
z	0.2218(25)	0.2258(24)	0.2156(26)	0.2187(24)	0.2198(21)	0.2129(32)
O2						
x	0.1173(17)	0.1142(16)	0.1104(17)	0.1132(16)	0.1139(14)	0.1102(22)
y	0.1726(8)	0.1712(7)	0.1705(8)	0.1722(7)	0.1718(6)	0.1705(11)
z	0.7274(26)	0.7248(24)	0.7224(26)	0.7179(24)	0.7194(20)	0.7185(31)
O3						
x	0.1078(19)	0.1072(16)	0.1080(19)	0.1084(17)	0.1119(15)	0.1128(24)
y	0	0	0	0	0	0
z	0.7226(40)	0.7126(38)	0.7186(39)	0.7183(36)	0.7201(31)	0.7042(49)
O4						
x	0.3605(16)	0.3609(14)	0.3561(16)	0.3590(14)	0.3587(11)	0.3552(18)
y	0.2500(7)	0.2489(6)	0.2478(7)	0.2465(6)	0.2465(6)	0.2451(9)
z	0.7826(30)	0.7814(29)	0.7820(31)	0.7846(30)	0.7867(25)	0.7796(39)
O5						
x	0.3537(15)	0.3496(14)	0.3516(20)	0.3442(17)	0.3443(15)	0.3438(25)
y	0.1414(6)	0.1404(6)	0.1365(7)	0.1352(6)	0.1335(6)	0.1307(9)
z	0.1296(31)	0.1174(30)	0.1132(32)	0.1022(29)	0.1002(25)	0.0953(38)
O6						
x	0.3401(17)	0.3388(15)	0.3368(19)	0.3429(17)	0.3407(15)	0.3427(24)
y	0.1141(6)	0.1126(6)	0.1132(7)	0.1155(6)	0.1163(5)	0.1154(8)
z	0.6249(34)	0.6147(32)	0.6043(34)	0.5954(31)	0.5913(26)	0.5884(42)
O7						
x	0.3461(20)	0.3445(18)	0.3435(20)	0.3371(19)	0.3367(16)	0.3443(26)
y	0	0	0	0	0	0
z	0.2784(42)	0.2804(39)	0.2805(40)	0.2932(38)	0.2942(32)	0.2974(50)
T1						
x	0.2822(9)	0.2830(9)	0.2815(10)	0.2803(9)	0.2816(8)	0.2810(13)
y	0.0855(4)	0.0849(4)	0.0858(4)	0.0854(4)	0.0843(3)	0.0840(5)
z	0.3082(17)	0.3052(17)	0.3013(18)	0.2966(17)	0.2979(14)	0.2992(23)
T2						
x	0.2888(11)	0.2882(10)	0.2880(11)	0.2892(10)	0.2881(9)	0.2869(15)
y	0.1722(4)	0.1715(4)	0.1714(4)	0.1709(4)	0.1704(3)	0.1713(5)
z	0.8113(18)	0.8081(17)	0.8061(19)	0.8065(16)	0.8032(14)	0.8041(24)
M1						
x	0	0	0	0	0	0
y	0.0873(7)	0.0884(6)	0.0870(7)	0.0873(6)	0.0868(6)	0.0830(9)
z	½	½	½	½	½	½
M2						
x	0	0	0	0	0	0
y	0.1768(6)	0.1765(6)	0.1763(7)	0.1768(6)	0.1767(5)	0.1743(9)
z	0	0	0	0	0	0
M4						
x	0	0	0	0	0	0
y	0.2794(4)	0.2799(4)	0.2776(4)	0.2775(4)	0.2773(3)	0.2729(6)
z	½	½	½	½	½	½

Note: M3 site fixed at $x = y = z = 0$; A site fixed at $x = z = 0$, $y = 1/2$ for all refinements except TREM 23-13 where it was removed from the structure. Isotropic displacement factors O1-O4 = 0.8; O5-O6 = 1.1; O7 = 1.2; T1-T2 = 0.4; M1-M3 = 0.6; M4 = 0.9; A = 2.3 Å².

TABLE 8. Selected interatomic distances (Å) for amphiboles listed in Table 6

	PARG 11-7	PARG 19-11	PARG 20-2	PARG 21-2	PARG 18-3	TREM 23-13
T1-O1	1.63(2)	1.62(2)	1.60(2)	1.61(2)	1.58(1)	1.52(2)
T1-O5	1.66(2)	1.66(2)	1.63(2)	1.61(2)	1.61(2)	1.61(2)
T1-O6	1.69(2)	1.66(2)	1.62(2)	1.63(2)	1.62(1)	1.60(2)
T1-O7	1.68(1)	1.66(1)	1.67(1)	1.64(1)	1.62(1)	1.64(1)
<T1-O>	1.67	1.65	1.63	1.62	1.60	1.59
T2-O2	1.63(2)	1.66(2)	1.69(2)	1.67(2)	1.65(2)	1.68(2)
T2-O4	1.59(2)	1.59(1)	1.55(2)	1.54(1)	1.55(1)	1.51(2)
T2-O5*	1.72(2)	1.68(2)	1.70(2)	1.65(2)	1.66(1)	1.66(2)
T2-O6	1.61(2)	1.64(2)	1.65(2)	1.68(2)	1.66(2)	1.71(2)
<T2-O>	1.64	1.64	1.65	1.63	1.63	1.64
M1-O1 (x2)	2.06(1)	2.05(1)	2.09(2)	2.05(1)	2.08(1)	2.14(2)
M1-O2 (x2)	2.09(2)	2.05(2)	2.04(2)	2.06(1)	2.07(1)	2.09(2)
M1-O3 (x2)	2.07(1)	2.07(1)	2.07(1)	2.08(1)	2.09(1)	2.01(2)
<M1-O>	2.08	2.06	2.06	2.06	2.09	2.08
M2-O1 (x2)	2.13(1)	2.13(1)	2.12(2)	2.13(1)	2.17(1)	2.11(2)
M2-O2† (x2)	2.08(2)	2.06(2)	2.04(2)	2.08(2)	2.07(1)	2.05(2)
M2-O4‡ (x2)	2.02(1)	2.04(1)	2.08(2)	2.08(1)	2.08(1)	2.16(2)
<M2-O>	2.08	2.08	2.08	2.09	2.10	2.10
M3-O1 (x4)	2.07(1)	2.10(1)	2.07(1)	2.07(1)	2.08(1)	2.12(2)
M3-O3† (x2)	2.03(2)	2.07(2)	2.04(2)	2.04(2)	2.05(2)	2.13(3)
<M3-O>	2.06	2.09	2.06	2.06	2.07	2.12
M4-O2 (x2)	2.39(1)	2.41(1)	2.37(2)	2.35(1)	2.36(1)	2.30(2)
M4-O4‡ (x2)	2.35(2)	2.34(2)	2.35(2)	2.33(2)	2.34(1)	2.32(2)
M4-O5‡ (x2)	2.54(1)	2.60(1)	2.67(1)	2.75(1)	2.78(1)	2.88(2)
M4-O6‡ (x2)	2.67(2)	2.68(2)	2.68(2)	2.60(2)	2.60(1)	2.65(2)
<M4-O>	2.49	2.50	2.52	2.51	2.52	2.54

Note: Values in < > are mean values.
* $x, y, 1 + z$.
† $x, y, -1 + z$.
‡ $\frac{1}{2} - x, \frac{1}{2} - y, 1 - z$.

do not strictly adhere to this simple binary join but display a small and probably non-linear enrichment in the MC component. Although the precision of electron-microprobe analysis of the small amphibole grains produced in this study does not allow direct proof of this, the modal abundances of the accessory phases (Table 5) support this hypothesis. Shown in Figure 9 are the modal variation in plagioclase and clinopyroxene coexisting with amphibole in the four bulk compositions that have ~80 mol% PG and which intersect the tremolite-pargasite join in the region that is most difficult to obtain syntheses. With increasing MC component, the amount of clinopyroxene steadily decreases from 6 to 0 wt% and the plagioclase decreases from about 2.5 to 1 wt%, such that PARG 19-11 has just reached the point of Ca-Mg saturation.

Figure 10 illustrates both the extent of MC enrichment observed for amphiboles formed in this study as well as the *P-T* range needed for optimal yields and any modifications made to the starting mixtures (addition of silica or treatment in NaOH solution). The MC enrichment is probably not linear within the TR-PG-MC system but rather reaches a maximum near the middle of the tremolite-pargasite join. As with tremolite (e.g., Maresch et al. 1994), the origin of the Mg enrichment could be due wholly or in part to the presence of wide-chain and Mg-rich "biopyriboles." Resolution of this issue requires a detailed TEM investigation of these materials, which is beyond the scope of the present study. Because MC solid solution in tremolite is clearly possible (e.g., Zimmerman et al. 1996; Bozhilov 1997) and previous TEM studies of synthetic pargasite have indicated few wide-chain defects (e.g., Welch et al. 1994), we conclude that MC solid solution plays a genuine role for amphiboles along the tremolite-pargasite join thus precluding formation of end-member compositions.

As mentioned above, electron-microprobe analysis indicated a slight excess of Na in amphiboles synthesized from mixtures with approximately 80 mol% PG, or Al(T) of 2.4, regardless of whether or not the samples were synthesized in a NaOH solution or H_2O. A similar observation is obtained from the Rietveld refinements (Table 6) where the Na content of these samples is found to be slightly higher than expected. Please note that the Rietveld refinement is *completely independent* of any results obtained with the electron microprobe. There is excellent agreement between the electron microprobe and Rietveld refinement analysis of the Na content as shown in Figure 11.

At present we can say relatively little about the substitution of cations into sites other than the A-site owing to the inherently lower precision of interatomic distances obtained from Rietveld vs. single-crystal refinements. There is a noticeable increase in the mean T1-O atomic distance compared to the nearly constant mean T2-O distance with increasing PG content (Table 8). This suggests a preferential substitution of Al^{3+} (radius = 0.39 Å, Shannon 1976) for Si^{4+} (radius = 0.26 Å) into the T1 site, as is commonly observed for amphiboles.

The unit-cell dimensions (Fig. 12) and volumes (Fig. 13) of the amphiboles formed in this study show a peculiar pattern. The amphiboles formed along the PCb-TCb join in pure H_2O (diamonds in Fig. 13), appear to have systematically lower volumes than those along the PCa-TCa join (circles). The squares indicate amphiboles formed in the presence of NaOH

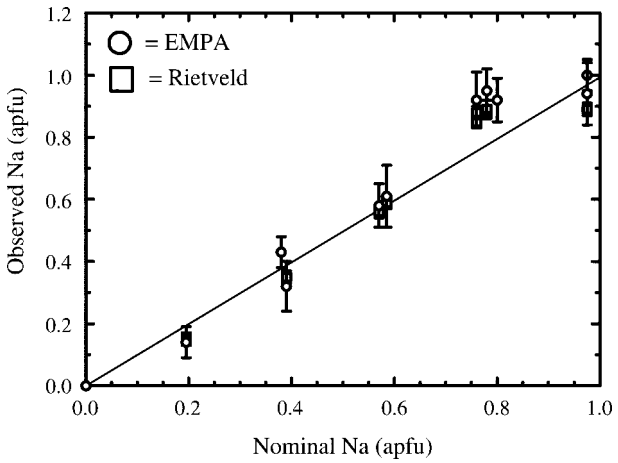

FIGURE 11. Observed vs. nominal Na content of amphiboles formed in this study as determined by electron microprobe analysis (circles) as well as by XRD Rietveld structure refinement (squares). Solid line represents perfect correlation.

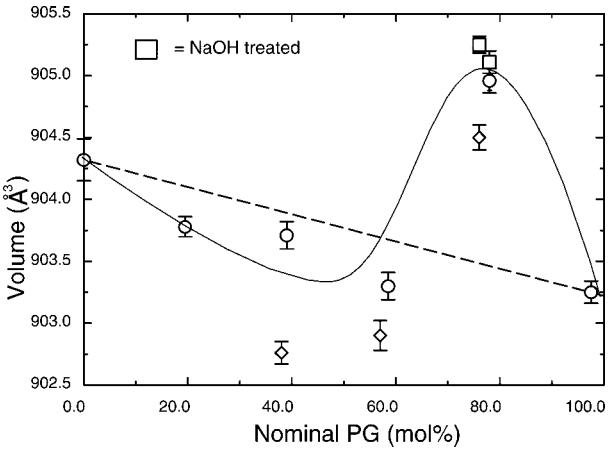

FIGURE 13. Unit-cell volumes of amphiboles formed in this study. Symbols are the same as in Figure 12. The dashed line is drawn between the end-member volumes for illustrative purposes whereas the sigmoidal curve is an approximate fit to the circles. Note the prominent increase in volume at about 80 mol% PG.

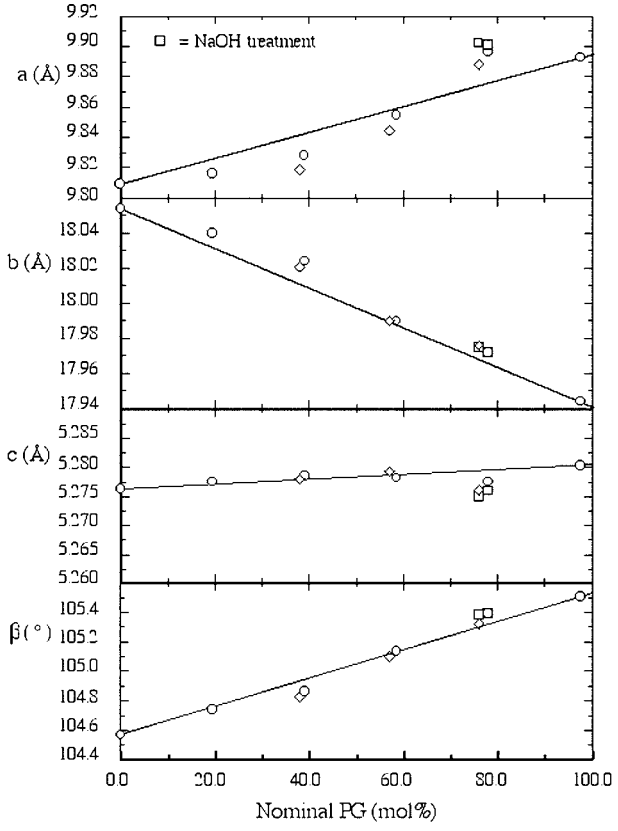

FIGURE 12. Unit-cell dimensions of amphibole formed in this study. Circles are for amphiboles formed along the PCa-TCa join, diamonds are for amphiboles formed along the PCb-TCb join, and squares indicate amphiboles formed in a 0.25 *m* NaOH solution. The straight lines drawn between the end-members are simply shown for illustrative rather than interpretive purposes and are *not* linear regressions to the data.

solutions. In Figure 13, the unit-cell volumes of the amphiboles could be interpreted as either having a sigmoidal pattern, if one places complete confidence in the end-member volumes as shown here, or as being essentially linear for all but the 80 mol% PG samples. Regardless of how one views the data in Figure 13, it is stressed here that the abnormally high volumes for the 80 mol% PG samples is not an artifact based on (1) the reproducibility of these volumes and (2) the similarity in this trend observed both for amphiboles formed within the TR-PG-MC ternary as well as those formed from bulk compositions strictly on the TR-PG join (bottom half of Table 6). The difficulty in forming amphiboles with ~80 mol% PG, their unusually high Na contents, and their unusually large volumes are certainly interrelated but in a manner that is not well understood at present.

Considerable attention was given to discerning the presence of amphibole immiscibility in the synthesis products of this study, as a wide miscibility gap was reported by Oba (1980) at 1 kbar. Although the present study focuses on the crystallochemical rather than phase-equilibrium properties of amphiboles, there was no evidence for amphibole immiscibility observed here, neither in terms of a bimodal distribution in amphibole chemical analyses nor as a two-amphibole XRD pattern from a single bulk composition (especially in the region of the 151 and $\bar{3}31$ reflections). An attempt was made to replicate the results of Oba (1980) by treating the bulk composition of PARG 16 (~60 mol% PG) at 790 °C and 1 kbar for 2116 hours (89 days), conditions that are well inside the 1 kbar miscibility gap reported by Oba (1980). Despite the relatively poor amphibole yield (~70 wt%), with coexisting clinopyroxene, plagioclase, and forsterite, the XRD pattern in the range of the 151 and $\bar{3}31$ reflections were sufficiently free of interfering peaks to show that the peak profiles were best modeled as a single amphibole.

Even though a miscibility gap has not been observed in this

study, its existence for natural hornblendes appears real in view of the compelling TEM evidence for actinolite-hornblende exsolution reported by Smelik et al. (1991). Our volume-composition data places some constraints on the placement of this gap in *P-T*-composition space. For the volume-composition relationships, a positive deviation from ideal mixing would imply decreasing miscibility with increasing pressure, whereas a negative deviation would imply increasing miscibility with increasing pressure. Again referring to Figure 13, if one accepts the "sigmoidal" interpretation of the volume data, then it is possible to derive a negative deviation in cell volumes for amphiboles at about 50 mol% PG, as was done by Oba (1980), and therefore deduce a miscibility gap that closes off with increasing pressure. However, the cell volumes near the 80 mol% PG composition clearly lie above any ideal-mixing trend, especially if one simply fits a straight line to all but the 80 mol% PG data, and therefore imply a tendency to unmix with increasing pressure. Although the compositions of natural coexisting actinolite-hornblende pairs are, if anything, shifted more toward tremolite than pargasite (Zingg 1996), the implications from this study are that exsolution would initiate first for pargasitic amphiboles with increasing pressure. Indeed, this may provide a test for discerning whether coexisting amphiboles are the result of exsolution as opposed to an overgrowth or discontinuous reaction process.

ACKNOWLEDGMENTS

We gratefully acknowledge financial support from NSF grants EAR-9316079 and EAR-9628212. Thanks are also given to W.H. Blackburn for assistance with the microprobe analyses.

REFERENCES CITED

Bégin, N.J. and Carmichael, D.M. (1992) Textural and compositional relationships of Ca-amphiboles in metabasites of the Cape Smith belt, northern Québec: Implications for a miscibility gap at medium pressure. Journal of Petrology, 33, 1317–1343.

Boyd, F.R. (1959) Hydrothermal investigations of amphiboles. In P.H. Abelson, Ed., Researches in Geochemistry, p. 377–396. Wiley, New York.

Bozhilov, K.N. (1997) Transmission electron microscopy study of crystal growth, solid solution, and defect formation: hollandite and synthetic tremolite. PhD Thesis, Johns Hopkins University.

Charles, R.W. (1980) Amphiboles on the join pargasite-ferropargasite. American Mineralogist, 65, 996–1001.

Giblin, L.E., Blackburn, W.H., and Jenkins, D.M. (1993) X-ray continuum discrimination technique for the energy dispersive analysis of fine particles. Analytical Chemistry, 65, 3576–3580.

Gillis, K.M., Thompson, G., and Kelley, D.S. (1993) A view of the lower crustal component of hydrothermal systems at the mid-Atlantic ridge. Journal of Geophysical Research (B), 98, 19,597–19,619.

Graham, C.M., Maresch, W.V., Welch, M.D., and Pawley, A.R. (1989) Experimental studies on amphiboles: A review with thermodynamic perspectives. European Journal of Mineralogy, 1, 535–555.

Hawthorne, F.C. (1995) Entropy-driven disorder in end-member amphibole. Canadian Mineralogist, 33, 1189–1204.

Hawthorne, F.C. and Grundy, H.D. (1976) The crystal chemistry of the amphiboles: IV. X-ray and neutron refinements of the crystal structure of tremolite. Canadian Mineralogist, 14, 334–345.

Jenkins, D.M. (1987) Synthesis and characterization of tremolite in the system H_2O-CaO-MgO-SiO_2. American Mineralogist, 72, 707–715.

Jenkins, D.M. and Hawthorne, F.C. (1995) Synthesis and Rietveld refinement of amphibole along the join $Ca_2Mg_5Si_8O_{22}F_2$-$NaCa_2Mg_4Ga_3Si_6O_{22}F_2$. Canadian Mineralogist, 33, 13–24.

Kamineni, D.C. (1986) A petrochemical study of calcic amphiboles from the East Bull Lake anorthosite-gabbro layered complex, district of Algoma, Ontario. Contributions to Mineralogy and Petrology, 93, 471–481.

Lager, G.A., Jorgensen, J.D., and Rotella, F.J. (1982) Crystal structure and thermal expansion of a-quartz SiO_2 at low temperatures. Journal of Applied Physics, 53, 6751–6756.

Lee, S.R. and Cho, M. (1995) Tectonometamorphic evolution of the Chuncheon amphibolite, central Gyeonggi massif, South Korea. Journal of Metamorphic Geology, 13, 315–328.

Levien, L. and Prewitt, C.T. (1981) High-pressure structural study of diopside. American Mineralogist, 66, 315–323.

Liang, J.J. and Hawthorne, F.C. (1994) Characterization of fine-grained mixtures of rock-forming minerals by Rietveld structure refinement: olivine and pyroxene. Canadian Mineralogist, 32, 541–552.

Lindsley, D.H. and Dixon, S.A. (1976) Diopside-enstatite equilibria at 850 °C to 1400 °C, 5 to 35 kbar. American Journal of Science, 276, 1285–1301.

Luth, W.C., Martin, R.F., and Fenn, P.M. (1974) Peralkaline alkali feldspar solvi. In W.S. MacKenzie and J. Zussman, Eds., Feldspars, p. 297–372. Manchester University Press, Manchester, U.K.

Maresch, W.V., Czank, M., and Schreyer, W. (1994) Growth mechanisms, structural defects and composition of synthetic tremolite: what are the effects on macroscopic properties? Contributions to Mineralogy and Petrology, 118, 297–313.

Oba, T. (1980) Phase relations int he tremolite-pargasite join. Contributions to Mineralogy and Petrology, 71, 247–256.

Oba, T. (1990) Experimental study on the tremolite-pargasite join at variable temperatures under 10 kbar. Proceedings of the Indian Academy of Science, 99, 81–90.

Oba, T. and Yagi, K. (1987) Phase relations on the actinolite-pargasite join. Journal of Petrology, 28, 23–36.

Oberti, R., Hawthorne, F.C., Ungaretti, L., and Cannillo, E. (1995) $^{[VI]}$Al disorder in amphiboles from mantle peridotites. Canadian Mineralogist, 33, 867–878.

Pawley, A.R., Graham, C.M., and Navrotsky, A. (1993) Tremolite-richterite amphiboles: Synthesis, compositional and structural characterization, and thermochemistry. American Mineralogist, 78, 23–35.

Raudsepp, M., Turnock, A.C., and Hawthorne, F.C. (1991) Amphibole synthesis at low pressure: what grows and what doesn't. European Journal of Mineralogy, 3, 983–1004.

Schumacher, R. (1991) Compositions and phase relations of calcic amphiboles in epidote- and clinopyroxene-bearing rocks of the amphibolite and lower granulite facies, central Massachusetts, USA. Contributions to Mineralogy and Petrology, 108, 196–211.

Sharma, A. (1996) Experimentally derived thermochemical data for pargasite and re-investigation of its stability with quartz in the system Na_2O-CaO-MgO-Al_2O_3-SiO_2-H_2O. Contributions to Mineralogy and Petrology, 125, 263–275.

Shannon, R.D. (1976) Revised effective ionic radii and systematic studies of interatomic distances in halides and chalcogenides. Acta Crystallographica, A32, 751–767.

Smelik, E.A., Nyman, M.W. and Veblen, D.R. (1991) Pervasive exsolution within the calcic amphibole series: TEM evidence for a miscibility gap between actinolite and hornblende in natural samples. American Mineralogist, 76, 1184–1204.

Solberg, T.N., Abrecht, J., and Hewitt, D.A. (1981) Graphical procedures for the refinement of electron microprobe analysis of fine-grained particles. In R. H. Geiss, Ed., Microbeam Analysis-1981, p. 160–162. San Francisco Press, California.

Welch, M.D., Kolodziejski, W., and Klinowski, J. (1994) A multinuclear NMR study of synthetic pargasite. American Mineralogist, 79, 261–268.

Wenk, H.R., Joswig, W., Tagai, T., Korekawa, M., and Smith, B.K. (1980) The average structure of An 62-66 labradorite. American Mineralogist, 65, 81–95.

Young, R.A., Sakthivel, A., Moss, T.S., Paiva-Santos, C.O. (1994) User's guide to program DBWS-9411, 60 p. Georgia Institute of Technology, Atlanta, Georgia.

Yang, H. and Evans, B.W. (1996) X-ray structure refinements of tremolite at 140 and 295 K: Crystal chemistry and petrologic implications. American Mineralogist, 81, 1117–1125.

Zimmermann, R., Heinrich, W., and Franz, G. (1996) Tremolite synthesis from $CaCl_2$-bearing aqueous solutions. European Journal of Mineralogy, 8, 767–776.

Zingg, A.J. (1996) Immiscibility in Ca-amphiboles. Journal of Petrology, 37, 471–496.

MANUSCRIPT RECEIVED JUNE 24, 1998
MANUSCRIPT ACCEPTED MAY 7, 1999
PAPER HANDLED BY CRAIG MANNING